Int. J. Electrochem. Sci., 12 **(2017)** 9565 – 9574, doi: 10.20964/2017.10.42

International Journal of
ELECTROCHEMICAL
SCIENCE
www.electrochemsci.org

Effect of HCO_3^- Concentration on the Corrosion Behaviour of X80 Pipeline Steel in Simulated Soil Solution

Fei Xie, Dan Wang[*]*, Chengxiang Yu, Yue Zong, Ming Wu*

Key Laboratory of Oil & Gas Storage and Transportation, College of Petroleum Engineering, Liaoning Shihua University, Fushun Liaoning, 113001, China.
[*]E-mail: wd841015@163.com

Received: 20 June 2017 / *Accepted:* 3 August 2017 / *Published:* 12 September 2017

In buried pipeline steel, soil environmental factors cause corrosion, which greatly affects the safe operation of pipe networks. The effects of HCO_3^- on the corrosion behaviour of X80 pipeline steel in Liaohe Oilfield simulated soil solution was investigated through potentiodynamic polarization and electrochemical impedance spectroscopy. The corrosion morphologies were observed by a metalloscope under different HCO_3^- concentrations. Accordingly, the polarization curves of the X80 pipeline steel exhibited the typical characteristics of activated passivation in the solution. With increasing HCO_3^- concentration, the corrosion rate of X80 steel increased and then decreased. The different anodic-current peaks obtained were caused by the property changes of the surface corrosion products of the electrode. When the HCO_3^- concentration was 0.2 mol/L, the metal corrosion reaction was disrupted. The surface corrosion phenomenon was not obvious and produced only few minor corrosion pits. In this case, the X80 pipeline steel showed the highest corrosion resistance, which was due to the widest passivation interval at this time, and the passivation film was complete and the densest. Thus, the best film protection was attained for the metal electrodes.

Keywords: X80 pipeline steel, bicarbonate ion, corrosion behaviour, Liaohe oilfield soil

1. INTRODUCTION

Long-distance oil and gas transportation have become increasingly common with rising energy demand. Therefore, using high-grade steel pipes has inevitably become the trend in developing pipelines for petroleum and natural gas [1−4]. Given its excellent weldability, high impact toughness, and high resistance to stress corrosion cracking, X80 steel is the preferred steel for manufacturing natural gas pipelines, and its application prospect is extensive [5–10]. Oil and gas pipelines are usually buried deeply and span long distances. Thus, these pipelines are easily affected by soil factors

throughout their service lives and may undergo corrosion. As a contributing factor, high soil HCO_3^- levels may cause varying degrees of corrosion in pipeline steel[11-15]. Domestic and foreign scholars have conducted research on the effect of the HCO_3^- io n on corrosion, but the views are not unified. In particular, Qiqi Gu [16] indicated that HCO_3^- ions first restrain and then promote corrosion in X80 pipeline steel, and steel matrix surface corrosion shifts from general to local with the increase of time in NaCl solution. Meanwhile, Yang Zhao et al. [17] showed that in $NaHCO_3$ solution, the passivation film of X100 and X80 steels generated n-type semiconductor characteristics. In the same study, the surface passivation film was generated through the control mixing mechanism of electromigration and dissolution–deposition. Zhang [18] proposed that the effect of Cl^- and SO_4^{2-} in HCO_3^- solution on metal corrosion rate is greater than that of Cl^- or SO_4^{2-} alone. However, scholars abroad and in northwest China study pipeline corrosion more intensively than in northeast China [19–22]. The Liaohe Oilfield is a major oilfield in China that supports the operations of the northeast oil and gas pipeline network. This oilfield is covered by typical alkaline soil with high HCO_3^- concentrations and erosion, which considerably threaten pipeline integrity. Therefore, this work studied the effect of HCO_3^- concentration on the corrosion behaviour of X80 pipeline steel in simulated soil solution as corrosion medium. The simulated soil solution was based on the soil 1 m underground of an oil and gas gathering and transportation company in the Liaohe Oilfield.

2. EXPERIMENTAL

2.1 Experimental materials

The test material was X80 pipeline steel (chemical composition in Table 1) provided by the China National Petroleum Corporation Pipe Research Institute. The X80 steel was processed into 10 mm × 10 mm × 2 mm square specimens by wire cutting. A copper wire was drawn by spot welding at the back of sample, leaving a 1 cm^2 working area. The remaining specimens were then coated in Polytetrafluoroethylene (PTFE) with epoxy resin. Before the experiment, the working electrode was polished from 80# to 1500# with SiC water sand paper and washed with distilled waterand anhydrous ethanol, and then dried.

2.2 Experimental medium

The test soil was gathered at about 1 m underground of the courtyard of an oil and gas transportation company in the Liaohe Oilfield. The samples were dried, ground and then mixed with deionised water at a 1:1 ratio to prepare the Liaohe Oilfield simulated soil solution. Physical and chemical data, such as the main components and pH value of the Liaohe Oilfield, were measured by ion chromatography and pH meter. The simulated soil solution was then prepared by analysing the pure drugs $NaHCO_3$, $CaCl_2$, $MgSO_4$, $MgCl_2$, NaCl and deionised water under the allocations shown in Table 2. The HCO_3^- levels were adjusted by setting the $NaHCO_3$ concentrations to 0.072, 0.12, 0.2, 0.3

and 0.5 mol/L. Prior to the experiment, the pH of the simulated solution was adjusted to 8.5 with 5% (volume fraction) NaOH solution and 5% (volume fraction) acetic acid.

2.3 Electrochemical experiment

Potentiodynamic polarization curves and alternating current (AC) electrochemical impedance spectroscopy (EIS) were tested by a PAR 2273 electrochemical work station and a conventional three-electrode system (X80 steel, Pt, and SCE were used as working, auxiliary, and reference electrodes, respectively). In the test, the working electrode was initially controlled at −1500 mV. The pre-polarization processing lasted for 3 min, the polarization curve scanning range was −1000 mV (vs. SCE) to 200 mV (vs. SCE) and the slow scanning rate was 0.5 mV/s. under the self-corrosion potential (E_{corr}), the EIS test frequency range was 10 mHz to 100 kHz, and the impedance amplitude was 10 mV. The surface morphology of the sample after polarization was observed under a Leica DM5200 metallographic microscope. The Origin7.5 software was used to fit the analysis of the polarization curves, and the experimental results were analysed by the ZsimpWin software. The experimental temperature was 298 K (25 °C). To ensure data accuracy, all the experiments were performed in triplicates with good repeatability.

Table 1. Chemical composition of X80 pipeline steel

C	Si	Mn	S	P	W	Ni	Nb	Ti	Cr	Cu	Al	Fe
0.06 %	0.08 %	1.87 %	0.005 %	0.006 %	0.01 %	0.16 %	0.044 %	0.01 %	0.03 %	0.26 %	0.03 %	residual

Table 2. Composition of simulated soil solution

Apellation	$NaHCO_3$	$CaCl_2$	$MgSO_4$	$MgCl_2$	NaCl
Use level (g/L)	2.731	0.364	0.120	0.306	2.254

3. RESULTS AND DISCUSSION

3.1 Electrochemical experiments

3.1.1 Polarization measurement

Figure 1 shows the polarization curves of the X80 steel in different HCO_3^- concentrations in the simulated soil solution. The changes in the corrosion potential of the X80 pipeline steel in the different solutions were not obvious and ranged from −800 mV to −700 mV (vs. SCE). By contrast, the anodic polarization curves varied greatly and showed passivation to different degrees. When the HCO_3^- concentration was 0.072 mol/L, the anodic polarization curve exhibited active–passive characteristics, and the passive interval was small (−600 mV to −500 mV [vs. SCE]). When the HCO_3^- level increased to 0.12 mol/L, two anodic current peaks, with the first peak lower than the second,

appeared in the anodic polarization curve. When the HCO_3^- concentration increased to 0.2 mol/L, the anodic polarization curves showed stable passivation until the potential exceeded −600 mV (vs. SCE), when the anode current density decreased sharply. Between −600 mV to −50 mV (vs. SCE), the anode current curve showed a passivation potential form, and beyond −50 mV (vs. SCE), the anode current increased rapidly and showed passivation characteristics. When the HCO_3^- continued to rise to 0.3 mol/L, the anodic polarization curves still showed stable passivation characteristics and maintained the passivity potential and current near to those in 0.2 mol/L HCO_3^-. When HCO_3^- evel reached 0.5 mol/L, two anodic current peaks, which corresponded to Fe and $FeCO_3$ dissolution, respectively, were prominent. Then the potentiodynamic polarization curves were fitted, and the results were shown in Table 3. The corrosion current density i_{corr} decreased first and then increased with rising HCO_3^- concentration. When the HCO_3^- level increased from 0.072 mol/L to 0.5 mol/L, the corrosive resistance of X80 pipeline steel increased gradually in the simulated solution, reached the peak at 0.2 mol/L and then decreased gradually. The corrosive resistance of X80 pipeline steel was the best when the HCO_3^- level was 0.2 mol/L in the solution.

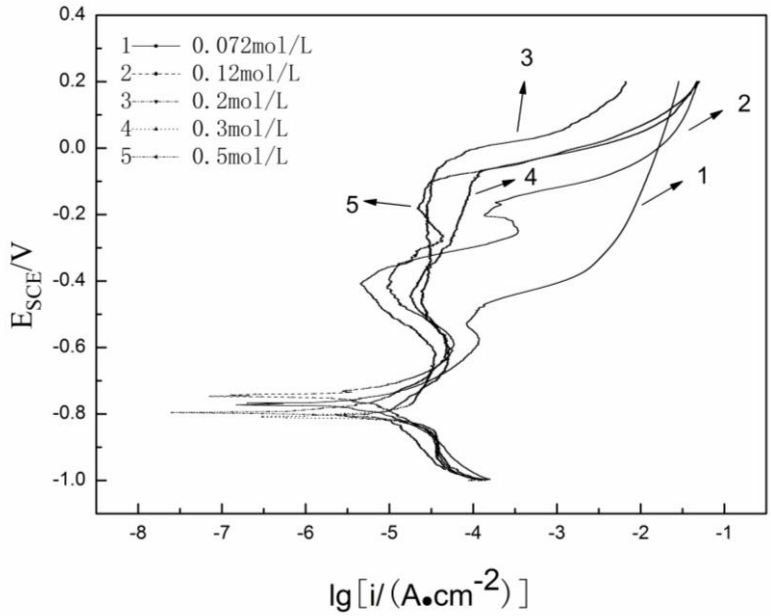

Figure 1. Dynamic potential polarization curves of X80 pipeline steel at different HCO_3^- ion concentrations in the simulated soil solution, which pH was 8.5.

Table 3. Corrosion potential and corrosion current density of X80 steel at different HCO_3^- ion concentration in the simulated soil solution.

HCO_3^- concentration/(mol/L)	Corrosion potential/V	Corrosion current density/(μA/cm^2)
0.072	-0.76	16.17
0.12	-0.74	9.91
0.2	-0.83	4.52
0.3	-0.81	6.79
0.5	-0.79	9.22

3.1.2 Electrochemical impendence spectroscopy (*EIS*)

Figure 2 presents an EIS diagram of X80 pipeline steel at different HCO_3^- concentrations in the simulated soil solution. The high-frequency region of the EIS diagram exhibits an obvious capacitance arc that became vestigial and incomplete in the medium- and low-frequency regions because of dispersion[23]. The larger diameter of the capacitance arc in EIS indicates better resistance against electrochemical corrosion. When the HCO_3^- concentration increased from 0.072 mol/L to 0.5 mol/L, the capacitance arc diameter increased first and then decreased. When the HCO_3^- concentration reached 0.2 mol/L, the capacitive arc attained the maximum diameter. This result implies that the resistance in the solution increased gradually and thus inhibited corrosive reaction when the HCO_3^- rose from 0.072 mol/L to 0.2 mol/L. From 0.2 mol/L to 0.5 mol/L HCO_3^-, the corrosive resistance in solution decreased gradually and increasingly facilitated corrosive reaction. Hence, the corrosive resistance decreased gradually with increasing HCO_3^- concentration.

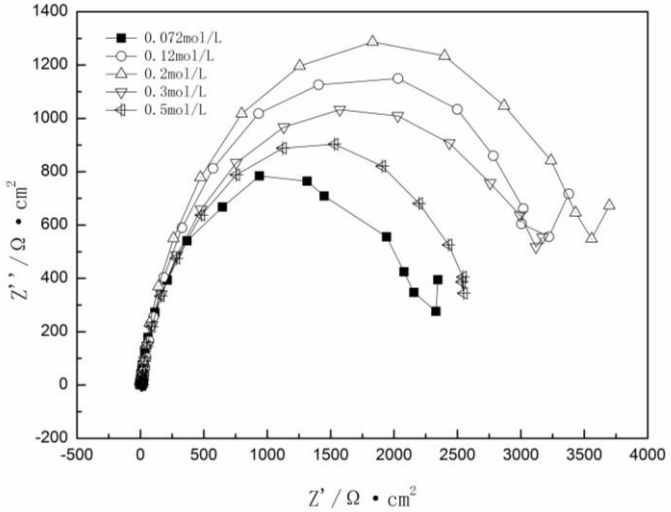

Figure 2. Nyquist diagram of X80 pipeline steel at different HCO_3^- ion concentration in the simulated soil solution, which pH was 8.5.

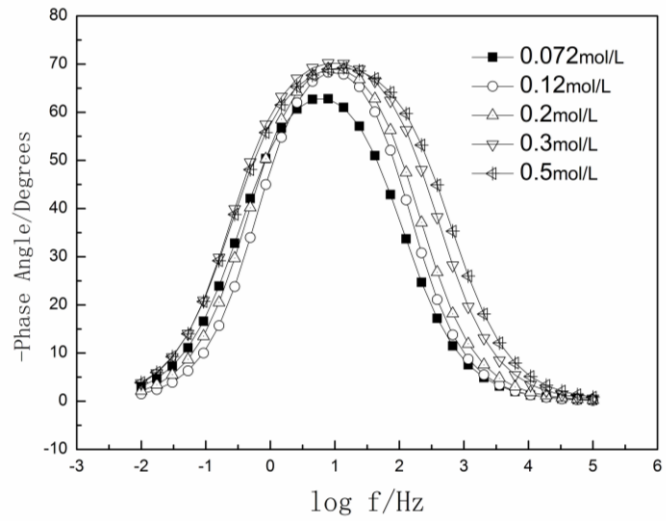

Figure 3. Bode curves of X80 pipeline steel at different HCO_3^- ion concentration in the simulated soil solution which pH was 8.5.

Figure 3 shows the Bode curves (curves of phase angle and frequency) of the X80 pipeline steel under different HCO_3^- levels in the simulated soil solution. From 0.072 mol/L to 0.5 mol/L HCO_3^-, the curve maintains only one peak, which indicates a time constant in the AC impedance spectrum. Given the characteristics of the self-system, Figure 4 displays the model of equivalent circuit used, in which R_s is the solution resistance between the working and reference electrodes, R_t is the charge-transfer resistance and C_{dl} is the double-layer capacitance on the electrode surface. In this equivalent circuit, the polarization resistance R_p is approximately equivalent to the charge-transfer resistance R_t. The electrochemical parameters were obtained by fitting with time variation (Table 4). Corrosion products formed, caused the electrode surface roughness and diffused. Thus, the element of the constant-phase angle was connected in series on the circuit and represented the element by Q to improve the fitting result. The was obtained through $Z_{CPE}=[j\omega]^{-n}/Y_0$, where ω is the angular frequency, Y_0 is the admittance constant and n is the diffusion index. The diffusion index n was related to the density and integrity of the product film[24]. Generally, the product film with an n of 0.5–1 is protected to a certain degree, and a larger diffusion index n indicates a stronger matrix protection performance by the corrosion product film[25]. In the fitting results, the charge-transfer resistance R_t increased constantly from 0.072 mol/L to 0.2 mol/L HCO_3^-. This finding suggests that the polarization resistance R_p increased continuously and impeded the corrosive reaction in solution. From 0.2 mol/L to 0.5 mol/L HCO_3^-, the R_t, and hence the R_p, decreased constantly in solution. Thus, the corrosive reaction could easily occur in solution, as similarly indicated by the polarization curves.

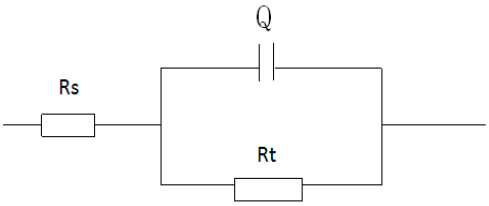

Figure 4. Equivalent circuit of X80 pipeline steel at different HCO_3^- ion concentration in the simulated soil solution.

Table 4. Fitting results of AC impedance

HCO_3^- concentration/(mol/L)	$R_s/(\Omega\cdot cm^2)$	CPE/(μF·cm^2)	*n*	$R_t/(\Omega\cdot cm^2)$
0.072	2339	2.372E^{-4}	0.8164	20.75
0.12	1867	1.630E^{-4}	0.8227	25.95
0.2	2470	1.692E^{-4}	0.8557	32.79
0.3	3334	2.081E^{-4}	0.8362	24.45
0.5	2782	2.469E^{-4}	0.8186	19.63

3.2 Corrosion morphology

The corrosion surface morphology of the X80 pipeline steel after polarization at different HCO_3^- levels is presented in Figure 5. Fig. 5 (a) presents a wide area of serious metal surface corrosion with many connected corrosion pits at 0.072 mol/L HCO_3^-. Meanwhile, the corrosion at 0.12 mol/L HCO_3^- (b) was high but less severe than in (a) and with small pit diameters of varying sizes. Compared with those in (b), the corrosion pits at 0.2 mol/L HCO_3^- (c) were significantly fewer, but the area of localised corrosion pits was obviously larger. Meanwhile, the overall corrosion morphology at 0.3 mol/L (d) was basically similar to that in (c), except for the higher number of corrosion pits in the former. Lastly, the overall corrosion morphology at 0.5 mol/L HCO_3^- (e), including the number and area of localised corrosion pits, increased substantially relative to that in (d). The above-mentioned corrosion trend suggests the protective effect of increasing HCO_3^- concentration on the metal through a passive film formed on the metal surface. However, as the reaction proceeded, corrosion ensued upon the rupture of the passive film and proceeded along the corrosion pits inwardly. Hence, large-diameter corrosion pits were formed.

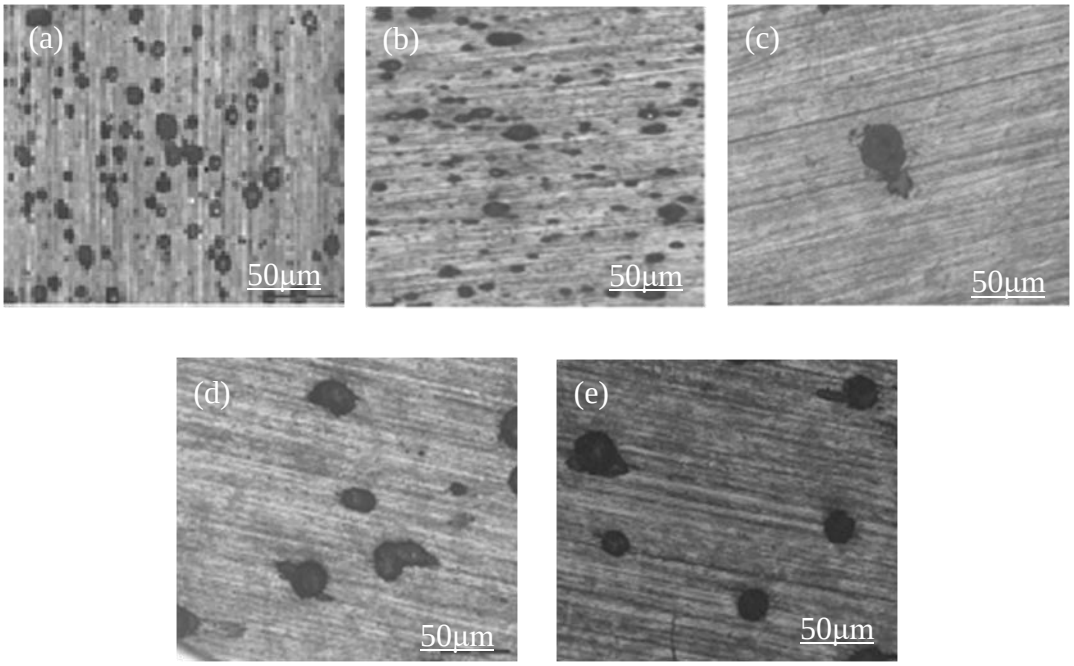

Figure 5. Surface corrosion morphology of X80 steel under different HCO_3^- ion concentration in the simulated soil solution, which pH was 8.5. HCO_3^- ion concentration were (a)0.072mol/L, (b)0.12mol/L, (c)0.2mol/L, (d)0.3mol/L, (e)0.5mol/L.

3.3 Mechanism analysis

The anodic-current peak of the potentiodynamic polarization curves of carbon steel at different HCO_3^- levels in solution might be related to the electrode potential, HCO_3^- concentration and solution pH[26,27]. That is, at increased electrode potential, HCO_3^- level and solution pH, the passive film easily formed and the stable passive potential range widened, but the passive film stability worsened.

Because the solution pH was constant throughout the experiment, the anodic peak of potentiodynamic polarization curve was related to the electrode potential and the HCO_3^- concentration.

At 0.072 mol/L HCO_3^-, only one anodic-current peak appeared on the polarization curves. The specimen surface only generated a thin layer of $Fe(OH)_2$ and $FeCO_3$ surface film[28]. This result was achieved because the HCO_3^- concentration was low, and HCO_3^- ionisation assumed the dominant role (Eq. 1). The numerous H^+ ions would be generated and consequently lowered the solution pH. However, the $Fe(OH)_2$ and $FeCO_3$ attained many defects and were unstable[29]; thus, the $Fe(OH)_2$ and $FeCO_3$ surface film may have dissolved in acidic medium. At this point, the activation–dissolution was reflected in the anode region of the polarization curve. The reactive equation is shown in Eqs. (1)–(5). According to the E-PH diagram of Fe-water system[30], when pH was 8.5 and the potential was between -0.7V to -0.8V in the simulated soil solution, Fe was relatively stable, and in alkaline media area, water acted as a reducing agent. Fe reacted with water to form $Fe(OH)_2$. This was consistent with the actual reflection.

$$HCO_3^- \rightarrow H^+ + CO_3^{2-} \quad (1)$$

$$Fe + H_2O \rightarrow Fe(OH)_2 + 2H^+ + 2e \quad (2)$$

$$Fe + HCO_3^- \rightarrow FeCO_3 + H^+ + 2e \quad (3)$$

$$Fe(OH)_2 + 2H^+ \rightarrow Fe^{2+} + 2H_2O \quad (4)$$

$$FeCO_3 + 2H^+ \rightarrow Fe^{2+} + CO_2 + H_2O \quad (5)$$

At 0.12 mol/L HCO_3^-, two anodic-current peaks on the anodic polarization curves were noted with increasing HCO_3^- level. The different current peaks represent the different Corrosion products produced at this time[31]. The dissolution of the iron matrix corresponded to the first anodic-current peak. The reactive equation is shown in Eq. (3). The $FeCO_3$ content in the solution increased but did not form a dense Corrosion product film. Thus, the dissolution of $FeCO_3$ at this point formed a second anode-current peak[32]. The reactive equation is shown in Eq. (6).

$$FeCO_3 + HCO_3^- \rightarrow Fe(CO_3)_2^{2-} + H^+ \quad (6)$$

At 0.2 mol/L HCO_3^-, most of the anode region of the electrode surface was occupied by HCO_3^-. At this point, hydrolysis of HCO_3^- ions resulted in large amounts of OH^- covering the specimen surface and forming a stable passive film. A larger passivation range indicates a higher corrosion resistance. The reactive equation is presented in Eqs. (7)–(9).

$$HCO_3^- + H_2O \rightarrow H_2CO_3 + OH^- \quad (7)$$

$$Fe + 2Fe(OH)_2 + 4OH^- \rightarrow Fe_3O_4 + 4H_2O + 4e \quad (8)$$

$$2Fe_3O_4 + H_2O \rightarrow 2Fe_2O_3 + 2H^+ + 2e \quad (9)$$

At 0.3 mol/L HCO_3^-, the surface passive film dissolved gradually, and the passive interval decreased. That is, the anode also began to dissolve gradually. This result was observed because solution conductivity is positively related to HCO_3^- concentration. Higher HCO_3^- concentration resulted in higher solution conductivity and hence, faster migratory velocity between the corrosion film and the solution interface[33,34]. Meanwhile, the high HCO_3^- concentration accelerated the dissolution of the $FeCO_3$ product film, which then released a large amount of Fe^{2+} into the solution and caused the surface film to further dissolve. Concurrently, partial HCO_3^- ionisation occurred (Eq. 1)

produced a large amount of H^+. As a result, some of the Fe_3O_4 and Fe_2O_3 passive films were dissolved by H^+ ions, decreasing the passive interval and the corrosive resistance.

At 0.5 mol/L HCO_3^-, the surface passive film continued to dissolve because of the adsorption of high HCO_3^- levels onto the point defects of the surface matrix film. This phenomenon impeded the migration of the free oxygen in the solution to the oxygenic vacancies[35,36]. Given the lack of oxygen, $FeCO_3$ film formation was inhibited. Meanwhile, the large number of Fe^{2+} retained on the surface matrix film did not participate in the reaction. As a result, the newly generated oxygenic vacancies could not be consumed in time. The passive interval continued to decrease, and the corrosive resistance also decreased.

4. CONCLUSIONS

(1) For simulated soil solutions with different HCO_3^- concentrations, anode polarization curves showed obvious passivation phenomenon. With increasing HCO_3^- concentration, the corrosion current density of X80 pipeline steel first decreased and then increased, and the metal's corrosion resistance first increased and then decreased. Moreover, the corrosion resistance was highest at 0.2 mol/L HCO_3^-.

(2) The corrosion product film plays a protective role on X80 steel. With increased HCO_3^- concentration, the corrosion product film generally thickened and was thoroughly compacted and led to enhanced matrix protection. However, when the HCO_3^- concentration exceeded 0.02 mol/L, the corrosion product film thinned and the corrosion resistance became poor due to increased solution conductivity and HCO_3^- adsorption.

ACKNOWLEDGEMENTS
This work was supported by the National Science Foundation of China (Grant No. 51604150 and 51574147), the Doctor Startup Foundation of Liaoning Province (Grant No. 201601324) and the Talent Scientific Research Fund of LSHU (No. 2016XJJ-032).

References

1. L. Wei, X.L. Pang, M. Zhou, K.W. Gao, *Corros. Sci*., 121 (2017) 57
2. X.G. Li, D.W. Zhang, Z.Y. Liu, Z. Li, C.W. Du, and C.F. Dong, *Nature*, 527 (2015) 441
3. Lerm S, Westphal A, Miethling G. R, *Extremophiles*, 17 (2003) 311
4. S.X. Li, S.R. Yu, H.L. Zeng, *Journal of Petroleum Science and Engineering*, 65 (2009) 162
5. H.X. Wan, D.D. Song, Z.Y. Liu, C.W. Du, X.G. Li, *Acta Metall. Sin*., 53 (2017) 575
6. L. Zhang, W.H. Cao, K.D. Lu, Z. Wang, Y.Y. Xing, *Int. J. Hydrogen Energy*., 42 (2017) 3389
7. D. Wang, F. Xie, M .Wu, G.X. Liu, Y. Zong, X. Li, *Metall. Mater. Trans. A*., 48A (2017) 2999
8. X.R. Guan, D.L. Zhang, J.J. Wang, Y.H. Jin, Y. Li, *J. Nat. Gas Sci. Eng.*, 37 (2017) 199
9. Y.F. Wang, G.X. Cheng, Y. Li, *Corros. Sci*., 111 (2016) 508
10. M.C. Yan, S. Yang, J. Xu, C. Sun, T.Q. Wu, C.K. Yu, W. Ke, *Acta Metall. Sin*., 52 (2016) 1133
11. W. Zhao, H. Zhang, Y. Zou, *Int. J. Electrochem. Sci*., 12 (2017) 679
12. F. F Eliyan, A. Alfantazi, *Corros. Eng., Sci. Technol*., 50 (2015) 178
13. Z.Y. Cui, Z.Y. Liu, L.W. Wang, C.W. Du, X.G. Li, *J. Mater. Eng. Perform.*, 24 (2015) 4400
14. W. Zhao, Y. Zou, D.X. Xia, Z.D. Zou, *Arch. Metall. Mater.*, 60 (2015) 1009
15. M. Zhu, C.W. Du, X.G. Li ,Z.Y. Liu, *Corros.*,70 (2014) 1181

16. Q.Q. Gu, L. Jian, X. L. Zhang, *Heat Treat. Met.*, 8(2015) 179
17. Y. Zhao, P. Liang, Y. H. Shi, *Journal of Chinese Society for Corrosion and Protection*, 6 (2013) 455
18. S.Y. Zhang, P. Liang, C.S. Hu, *Corros. Prot.*, 35 (2014) 14
19. Z.Y. Liu, W.R. Zheng, L.W. Wang, *J. Univ. Sci. Technol. Beijing*, 11 (2014) 1483
20. Q. Han, W. Li, H. Wang, *J. Mater. Eng. Perform.*, 24 (2016) 1.
21. M. Zhu, Z.Y. Liu, C.W. Du, *J. Mater. Eng.*, 43 (2015) 85
22. F. Xie, M. Wu, X. Chen, *Journal of Central South University (Science and Technology)*,44 (2013) 424
23. M. Wu, F. Xie, X. Chen, *Journal of Sichuan University(engineering science edition)*, 45 (2013) 185
24. H.C. Ma, Z.Y. Liu, C.W. Du, *Corros. Sci*., 100 (2015) 627
25. L. Fan, Z.Y. Liu, W.M. Guo, *Acta Metall. Sin*., 28 (2015) 866
26. Z.Y. Liu, X.G. Li, Y.F. Cheng, *Electrochim. Acta*, 60 (2012) 259
27. C. Zhang, Y.F. Cheng, *J. Mater. Eng. Perform.*, 19 (2010) 834
28. T.Q. Wu, M.C. Yan, D.C. Zeng, *Acta Metall. Sin*., 28 (2015) 93
29. L. Niu, Y.F. Cheng. *Appl. Surf. Sci*., 253 (2007) 8626
30. X.J Xie, H. Wang, P.G. Zou, L. Pan, *Journal of North China Electric Power*, 5(2011)23
31. J. Ding, Z. Lei, D. Li, *J. Mater. Sci*., 48 (2013) 3708
32. M. Zhu, C. Du, X. Li, *J. Mater. Eng. Perform.*, 23 (2014) 1358
33. B.Y. Fang, A. Atrens, J.Q. Wang, *J. Mater. Sci*., 38 (2003) 127
34. L. Fan, Z.Y. Liu, W.M. Guo, *Acta Metall. Sin*.,28 (2015) 866
35. M. Zhu, C. Du, X. Li, *J. Mater. Eng. Perform.*, 23 (2014) 1358
36. Marimuthu V., Kannoorpatti K., *Journal of Bio- and Tribo-Corrosion*, 2 (2016) 29